NUMERICAL SIMULATION OF UNSTEADY VISCOUS FLOW AROUND AIRSHIP USING VORTEX METHOD

Subagyo
UPT-LAGG, Badan Pengkajian dan Penerapan Teknologi
e-mail: cpbagyo@yahoo.com

ABSTRACT

The grid-less Vortex Method has been developed as the tool for the analysis of two-dimensional (2D) and three-dimensional (3D) complex flows in various engineering applications. In the present study, unsteady flows around a slightly complex geometry (bare hull of an airship and body of an airship) at angles incidence α= 10°, 20°, and 30° were investigated by using the vortex method for a high Reynolds number, Re = 3.9×10⁵. The flow-pattern, velocity field, coefficient of pressure distribution on the bare hull and the surface of the airship body, and the aerodynamic coefficient were obtained from numerical calculations. A comparison of the numerical results with the experimental observations showed a good agreement.

Keywords: *Vortex method, Unsteady flow, Aerodynamic coefficient*

ABSTRAK

Metode Vortex tanpa menggunakan kisi-kisi atau grid sudah dibangun sebagai alat untuk menganalisa aliran yang kompleks dua-dimensi (2D) dan tiga dimensi (3D) pada berbagai pemakaian di bidang keteknikan. Pada penelitian ini, aliran tidak tunak di sekitar geometri yang agak kompleks badan airship tanpa permukaan kontrol dan badan airship dengan permukaan kontrol pada **sudut serang** α= 10°, 20°, dan 30° disimulasikan dengan memakai metode vortex pada bilangan Reynolds yang tinggi, Re = 3.9×10⁵. Pola Aliran, medan kecepatan, koefisien distribusi tekanan di permukaan airship tanpa permukaan kontrol dan permukaan badan airship dengan permukaan kontrol, dan koefisien aerodinamika didapatkan dari perhitungan. Perbandingan hasil koefisien aerodinamika dengan pengamatan percobaan menunjukkan hasil yang bersesuaian.

Kata kunci: *Metoda vortex, Aliran tak tunak, Koefisien aerodinamika*

NOMENCLATURE

u   = velocity vector
ω   = vorticity
ρ   = air density
υ   = kinematic viscosity
ε   = core radius
C_p = pressure coefficient
C_x = drag forces in the body system
C_y = lift forces in the body system
C_{m_z} = moments in the body system
⁻   = average value
V   = volume of the airship body
$\mathbf{U}_\infty$ = Free stream velocity

$$C_{LV} = \frac{\overline{Cy}}{\frac{1}{2}\rho U_\infty^2 V^{\frac{2}{3}}} = \text{volumetric lift coefficient}$$

$$C_{DV} = \frac{\overline{Cx}}{\frac{1}{2}\rho U_\infty^2 V^{\frac{2}{3}}} = \text{volumetric drag coefficient}$$

$$C_{MV} = \frac{\overline{Cm_z}}{\frac{1}{2}\rho U_\infty^2 V} = \text{volumetric moment coefficient}$$

1   INTRODUCTION

In the last decade, airships have been in the spotlight again. Airships have a unique characteristics compared with other aircraft. An airship has very high efficiency and can stay alot for several days. Airships have been built for various civilian uses: for tourism, as stratospheric

platforms for communication support systems, as advertisement tools, for transportation, and so on. Military airships have been built for surveillance and transportation of large cargo.

Nowadays, research on and the development of airships are carried out using wind tunnels and computational fluid dynamics (CFD). Although CFD has matured in the last two decades, some challenges to improving its efficiency and accuracy for engineering applications still remain. Furthermore, regarding the application of CFD to unsteady flows around bluff bodies in two dimensions (2D) and three dimensions (3D), Bearman (P.W. Bearmen, 1998) and Lutz et al. (T. Lutz, P. Funk, A. Jacobi, and S.Wagner) pointed out that the flow near a bluff body wake is greatly affected by the presence of large coherent structures whose effect on the flow is not predicted well by using codes based on the Reynolds Averaged Navier-Stokes equations. Standard turbulence model also do not predict the effect of these structures on the flow.

After the successful work on the discontinuity of vorticity carried out by Rosenhead (L. Rosenhead, 1931) in 1931, vortex methods have been developed using computational techniques, notably by Chorin (A.J. Chorin, 1973), Leonard (A. Leonard, 1980), Sarpkaya (T. Sarpkaya, 1988) and Koumoutsakous and Leonard (T. Koumoutsakous, and A. Leonard, 1995). Kamemoto (K. Kamemoto, 1995) explained the wide range of attractive applications of the vortex method based on the Biot–Savart law.

In this paper, the vortex method developed by Ojima and Kamemoto (A. Ojima, and K. Kamemoto, 2000) for unsteady flows around a 3D body is used to analyze the unsteady flow around a slightly complex geometry. Recent work of Fukuda and Kamemoto (K. Fukuda and K. Kamemoto, 2004) indicates that the core spreading method may be used to analyze

unsteady flow in a wide range Reynolds number. The vortex method appears very attractive for simulation of unsteady and vortical flows around a body of complex geometry. This work shows that the present method can be used in the analysis and design of aircraft, vehicle and other engineering structures.

2   NUMERICAL METHOD

The flow phenomena in engineering problems can be described by Navier-Stokes equations. To get the solution of the velocity vector, u, v, w, and pressure, P, we derived the vorticity transport equation and pressure Poisson equation by taking the rotation and divergence of the Navier-Stokes equations. The vorticity transport equation can be written as,

$$\frac{\partial \boldsymbol{\omega}}{\partial t} + = \left(\boldsymbol{\omega} \cdot \vec{\nabla}\right)\mathbf{u} + \nu\nabla^2\boldsymbol{\omega} \left(\mathbf{u} \cdot \vec{\nabla}\right)\boldsymbol{\omega} \qquad (2\text{-}1)$$

where $\mathbf{u}$ is the velocity vector and ν the kinematic viscosity. The vorticity $\boldsymbol{\omega}$, is defined as

$$\boldsymbol{\omega} = \vec{\nabla} \times \mathbf{u} \qquad (2\text{-}2)$$

and the Poisson equation can be written as

$$\nabla^2 \mathrm{p} = -\rho\vec{\nabla}\left(\mathbf{u} \cdot \vec{\nabla}\mathbf{u}\right) \qquad (2\text{-}3)$$

The computational schemes to solve the vorticity transport equations and the Poisson pressure equations in this paper are the same as those described in Ref. (K. Fukuda and K. Kamemoto, 2004). A computational study is carried on modern type of airship called the LOTTE airship.

The computational panels are shown in Figure 2-1. The origin of the coordinate system coincides with the center of the airship. The axis coordinates x and z represent the direction along the stream and the direction along the span, respectively.
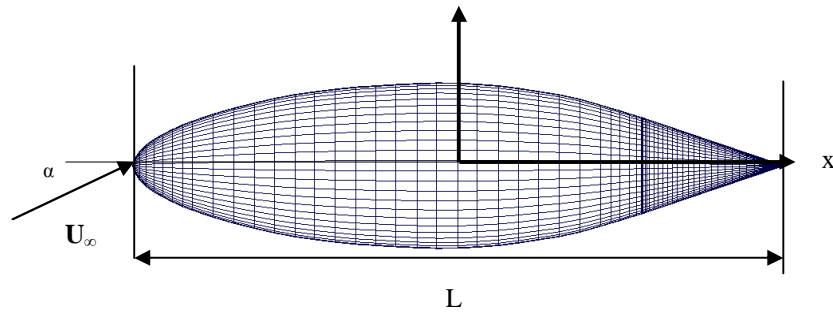
Side view (x-y plane) of the bare hull with non-dimensional length L=1.
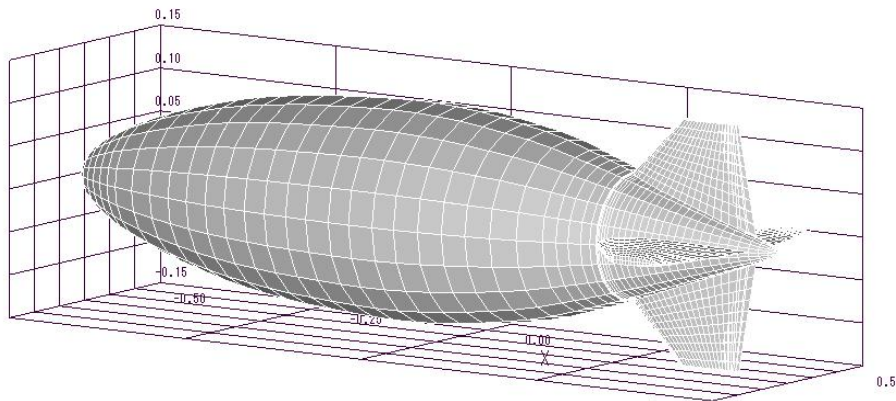
3D Perspective of the airship body

Figure 2-1: Computational panel of the bare hull and airship body for simulation

3   RESULTS

The experimental data reported in Ref. (T. Lutz, P. Funk, A. Jacobi, and S. Wagner, 2002) are for a modern airship of this decade. Our present study on the modern airship interests on the wake simulation; pressure distribution and aerodynamic force act to the bare hull and airship body.

The interesting aspect of a flow around a complex 3D geometry is the wake structure behind the body. The analysis of the aerodynamic forces at a high angle of attack could not be conducted very well without visualization of the wake shedding behind the body. In this study, the development of a vortical wake behind an airship body after its impulsive start at a constant speed in a fluid at rest is simulated with $Re=3.9\times10^5$, and an angle of incidence α = 10°, 20°, and 30°. The direction of the free stream velocity is from left to right in the direction of the x-axis. A total of 3100

panels of source and vortex strength are distributed on the surface of the airship body with the boundary condition satisfied at the surface. The time-step value, $\Delta tU_\infty/L$, is set equal to 0.05. Figure 3-1 shows a side view of an unsteady flow pattern around the body of the airship at non-dimensional time tU_∞/L = 2.5 at an angle of incidence α = 0°. At 0° the vortices are shed from the middle region of the body (x/L=0.0) downstream to the stern region. The wake behind the airship at this angle of incidence is periodic. The flows pattern is such that produces zero lift and drag. The stern region is always covered by vortices, and these are shed from the body of the airship.

The flow patterns obtained by simulation at an angle of attack of 20° are shown in Figures 3-2 – Figures 3-8. They indicate that the flows are fully separated turbulent flows. Figure 3-2   shows a side view of an unsteady flow pattern around the body of the airship at non-

dimensional time $tU_\infty/L=2.5$ at an angle of incidence of 20°. The major feature of the vortical wake structures behind the body of the airship at an angle incidence of 20° is pair of vortical wakes rolling up from the upper surface of the body of the airship at the rear seen in the flow pattern in the upper view in Figure 4-5. The **unsteady flow at an angle of incidence α = 20° around the bare hull and airship is shown in Figure 3-2 and Figure 3-3.**

Figure 3-3 shows that the fin of the airship has an effect on the shedding of the wake from the surface of the body. Further, the shedding of the vortex is observed at the tip of the horizontal fin in Figure 3-5. A detail of the flow pattern around the airship at an angle of **incidence α = 20° and Re = 3.9×10⁵** at time t = 2.5 is shown in Figure 3-6.

Vortex shedding comes from leeward surface form complex turbulence separated flow and through to the vertical tail of the airship. The horseshoes phenomenon is observed in the horizontal tail region; this is caused by vortex shedding from the tip of the fin of the airship in the downstream direction. The separated flow at the upper surface of the horizontal tail is also shown in Figure 3-6.

Interestingly, the separated flow phenomenon occurred along with the horseshoes flow (see also Figure 3-8). Figure 3-7 shows vortices on the surface of the body flowing adjacent to the horizontal tail and the lower part of the vertical tail. Separated flow is seen also to a lesser extent at the pressure side of the horizontal tail. The complex turbulent vortex flows at the upper part of the vertical tail are shown in Figure 3-6 and Figure 3-8; however, a few vortices that have been shed and carried by convection downstream at the lower part of the vertical tail are shown in the Figure 3-8 (see also Figure 3-7).
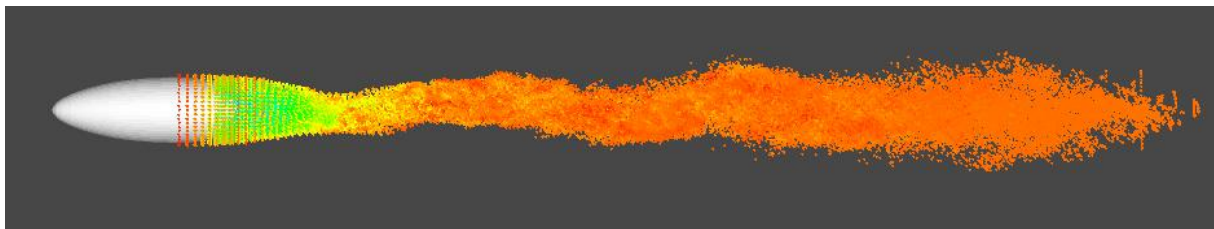

Figure 3-1:Instantaneous flow patterns represented by discrete vortices, Re=390000, t=2.5, x-y plane side view α=0°

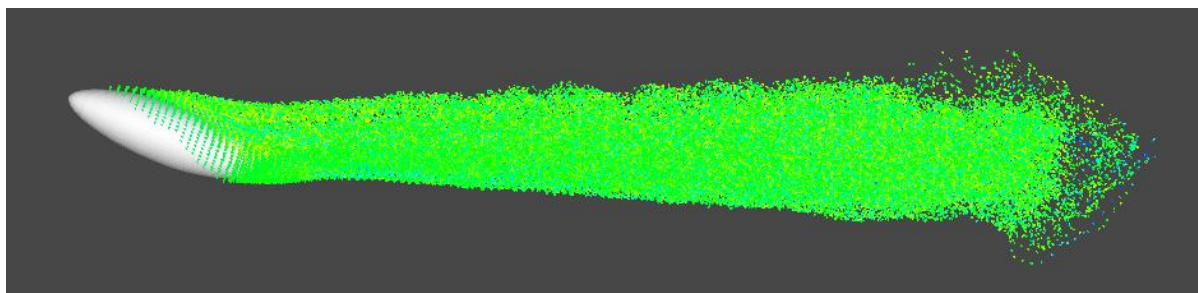Figure 3-2:Instantaneous flow patterns around the bare hull, Re=390000, t=2.5. x-y plane, side view α=20°
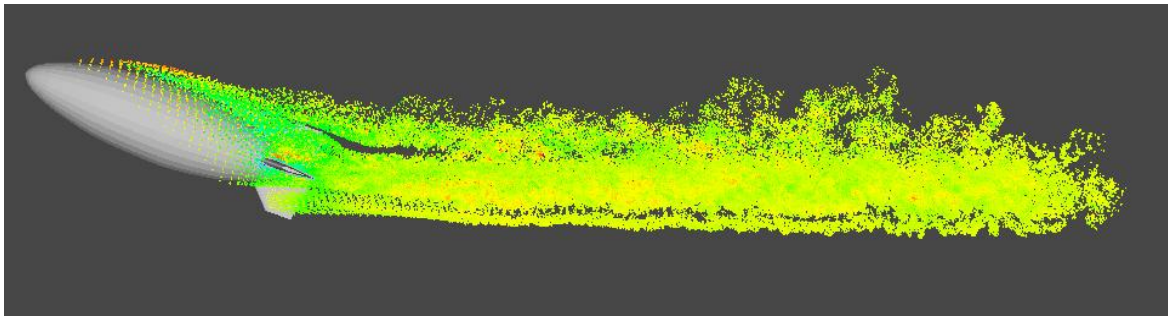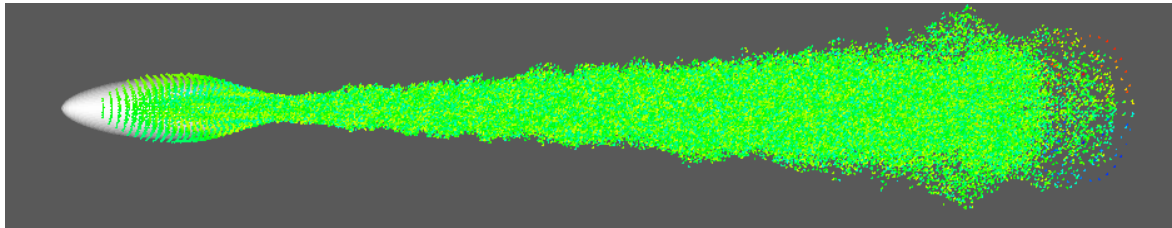
Figure 3-3:Instantaneous flow patterns around the airship, Re=390000, t=2.5. x-y plane, top view α=20°

Figure 3-4:Instantaneous flow patterns around the bare hull, Re=390000, t=2.5. x-z plane, top view α=20°
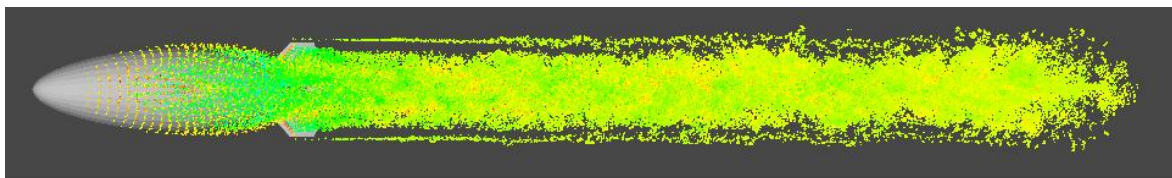

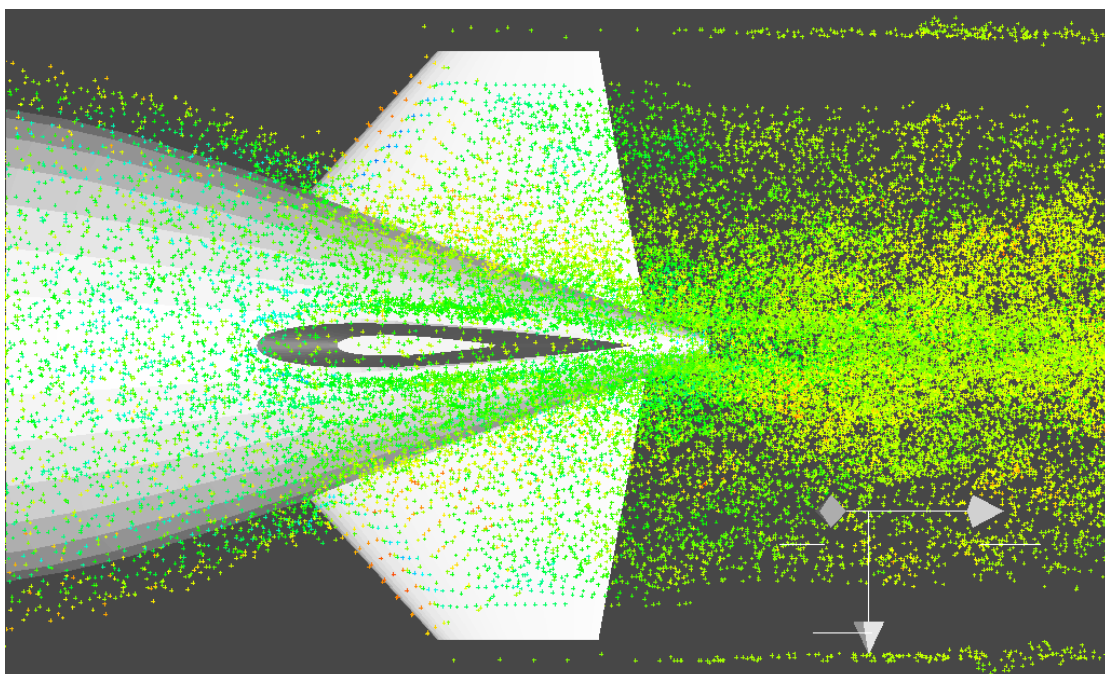Figure 3-5:Instantaneous flow patterns around the airship, Re=390000, t=2.5. x-z plane, top view α=20°

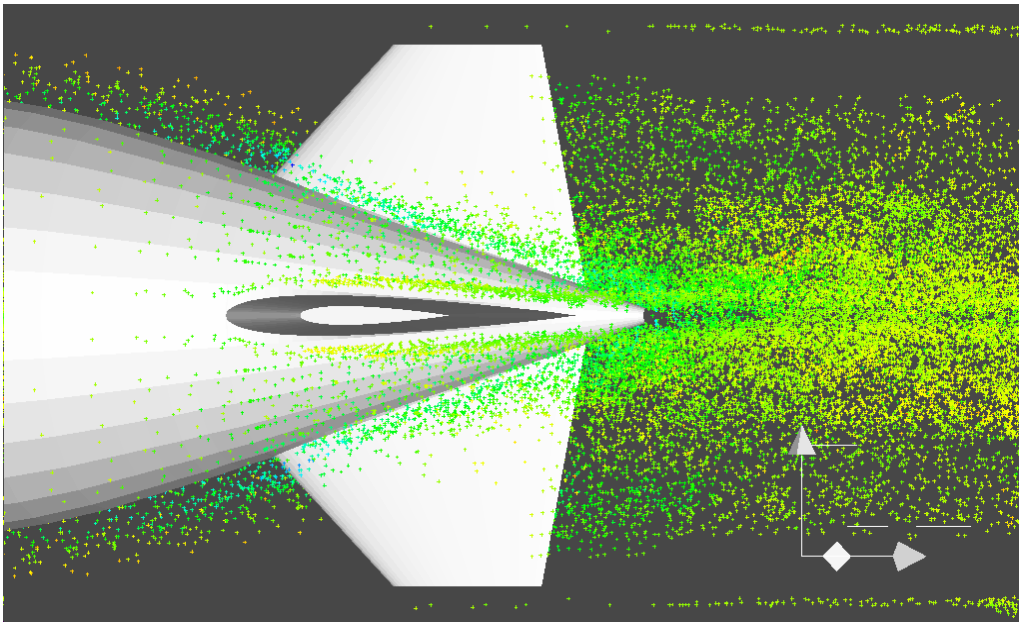Figure 3-6 Detail of the flow pattern, x-z plane, top view, Re=390000, t=2.5, α=20°

Figure 3-7: Detail of the flow pattern, x-z plane, bottom view, Re=390000, t=2.5, α=20°
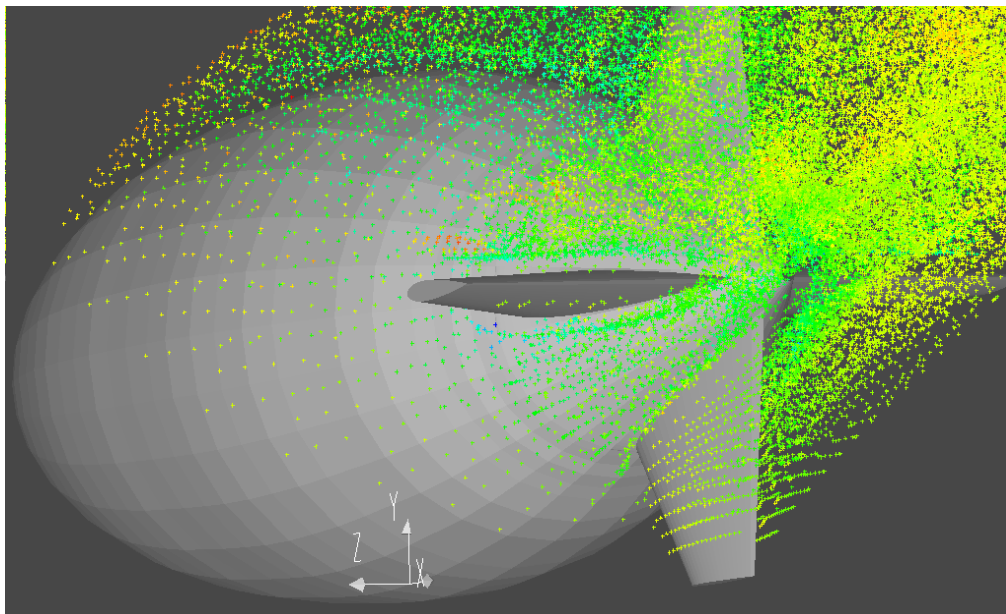
Figure 3-8: Perspective detail of the flow pattern Re=390000, t=2.5, α=20°

Figures 3-9 and Figure 3-11 show the velocity vector at the surface of the panel at a distance h from the surface of the bare hull at non-dimensional time $tU_\infty/L = 2.5$ at an angle of incidence 20° and Re = 3.9×10^5. The corresponding pressure distributions are shown in the Figures 3-13 and Figures 3-14. Figures 3-9 and Figures 3-11 show that some areas at the nose of the airship have a very low velocity (shown by the velocity vector in blue); corresponding to the stagnation-pressure value near the nose area of the surface of the airship shown in Figure 3-13 and Figures 3-14. We call the red spot in the 3D pressure distribution of the figure "the stagnation area" corresponding to the 2D term "stagnation point".

Figures 3-10 and Figure 3-12 show the velocity vector on the surface of the panel of the airship. The pressure distribution has changed a little because of the effect of the hull-fin configuration. At the upper part of the vertical fin, a low-velocity vector distribution is observed at the leading edge as well as near the nose region of the airship. The

pressure distributions of this condition are shown in Figure 3-15 and Figures 3-16. Figure 3-15 shows the stagnation area as a red spot at the leading edge of the vertical fin. A similar phenomenon is seen on the surface of the pressure side in Figure 3-16.
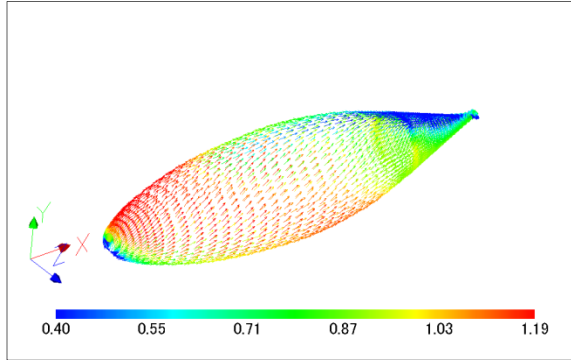

Figure 3-9: Velocity distributions at the upper-side outer boundary layer of the airship body surface
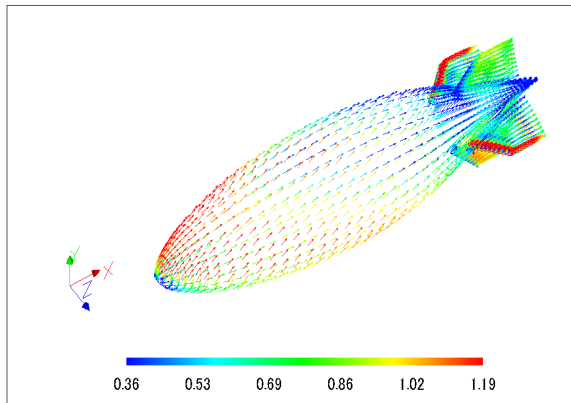

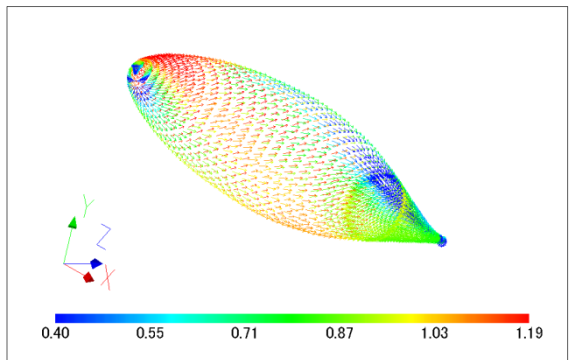Figure 3-10: Velocity distributions at the upper-side outer boundary layer of the airship body surface

Figure 3-11: Velocity distributions at the lower- side outer boundary layer of the airship body surface
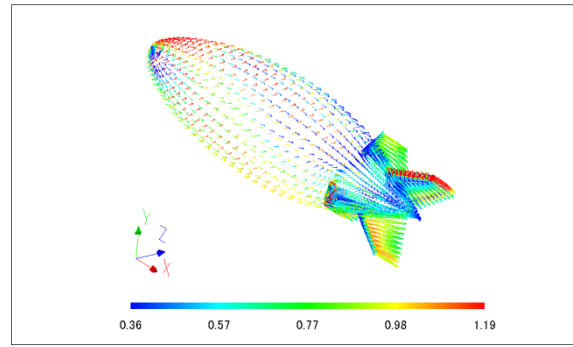

Figure 3-12: Velocity distributions at the lower- side outer boundary layer of the airship body surface

Figures 3-13 – Figures 3-16 show the instantaneous pressure distribution at non-dimensional time $tU_\infty/L = 2.5$ at an angle of incidence 20° and Re = 3.9×10^5. The red spot indicates the stagnation area of the flow. The pressure coefficient value varies from - 0.66 to 0.99. At the lower side, the value of the pressure coefficient is predominantly positive. On the upper surface, the value of the pressure coefficient is predominantly negative. Therefore a lift force is produced and acts on the bare hull and body of the airship.
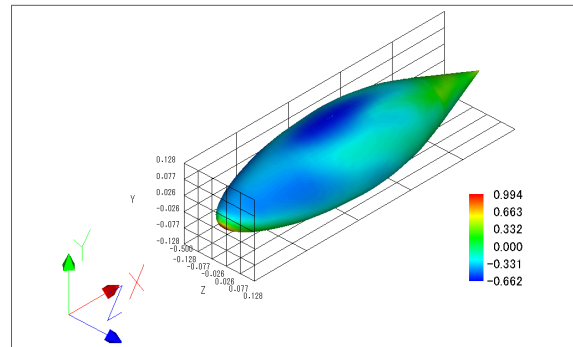

Figure 3-13: Pressure distributions at the upper-side bare hull surface
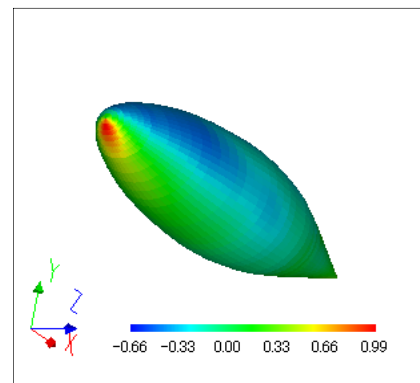

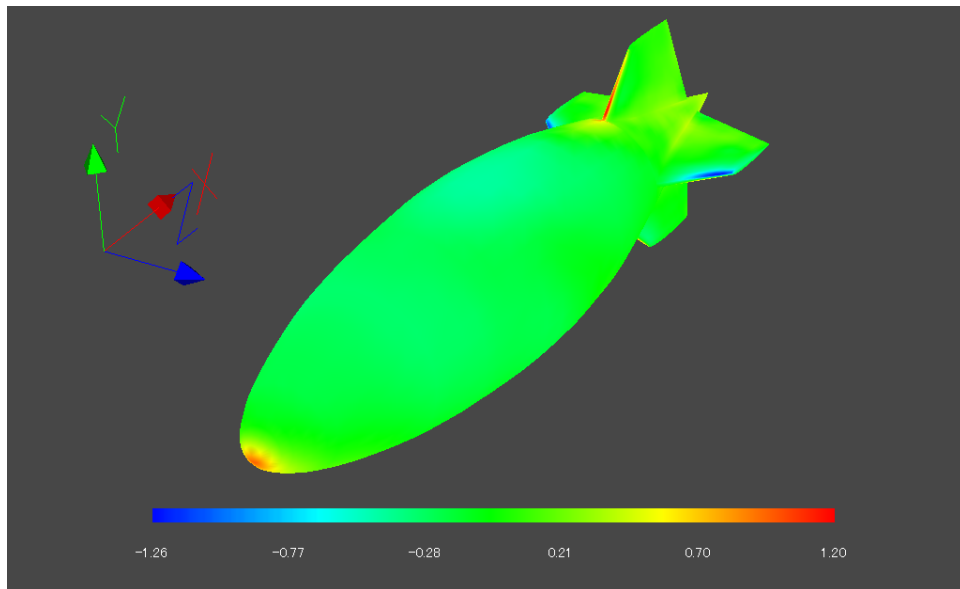Figure 3-14: Pressure distributions at the lower side bare hull surface

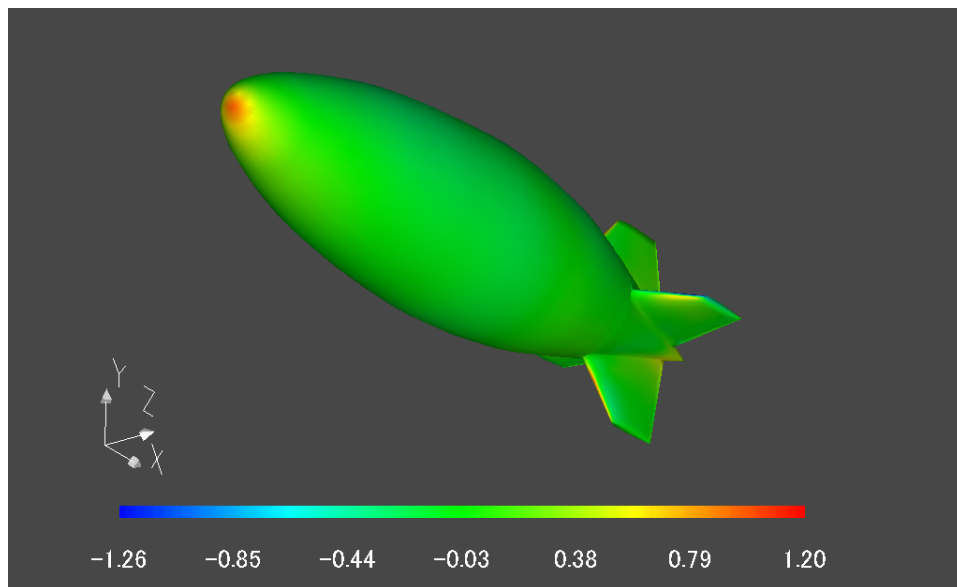Figure 3-15: Pressure distributions at the upper side of the airship surface

Figure 3-16: Pressure distributions at the lower side of the airship surface

Figure 3-17 – Figure 3-19 show a comparison of the time histories of the lift, drag and moment acting on the bare hull and airship at an angle incidence $\alpha = 20°$ and $Re = 3.9 \times 10^5$ in the body axis system. Figure 3-17 shows the lift force versus nondimensional time, tU_∞/L, for the bare hull and the airship. The lift force acting on the bare hull becomes stable at an average value $\overline{Cy} = 0.013$ at nondimensional time $tU_\infty/L = 0.5$. Whereas the lift force acting on the airship becomes stable at an average value $\overline{Cy} = 0.039$ at nondimensional time of about $tU_\infty/L = 0.25$.
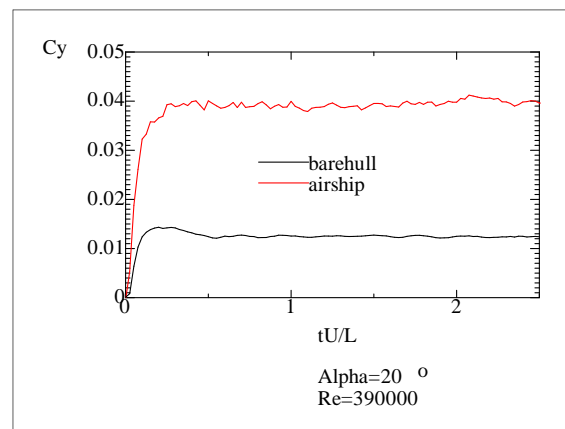

Figure 3-17: Time histories of lift force acts on the airship body at angle incidence $\alpha=20°$, $Re= 3.9 \times 10^5$
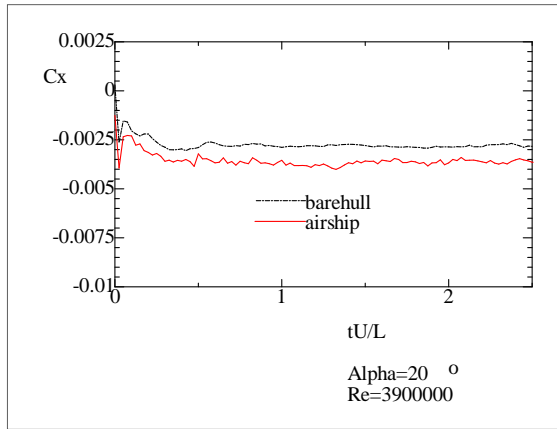
132

Figure 3-18: Time histories of drag force acts on the airship body at angle incidence α=20°, Re= 3.9x10⁵

Figure 3-19: Time histories of moment e acts on the airship body at angle incidence α=20˚, Re= 3.9x10⁵

Figure 3-18 shows the drag force versus nondimensional time, tU_∞/L, for the bare hull and the airship. The drag force acting on the bare hull becomes stable at an average value $\overline{Cx}$ = -0.00275 at nondimensional time tU_∞/L = 0.75. Whereas the drag force acting on the airship becomes stable at an average value $\overline{Cx}$ = -0.0035 at nondimensional time of about tU_∞/L = 0.6.

Figure 3-19 shows the moment versus nondimensional, time tU_∞/L, for the bare hull and the airship. The moment acting on the bare hull becomes stable at an average value $\overline{Cmz}$ = -0.015 at nondimensional time tU_∞/L = 0.5. Whereas the moment acting on the airship becomes stable at an average value $\overline{Cmz}$ = 0.0 at nondimensional time of about tU_∞/L = 0.

Furthermore, the volumetric lift, drag and moment coefficients are obtained by converting the values to the wind axis system respectively. The numerical calculations yield stable values for the lift, drag, and moment.

The average values of the lift, drag, and moment have been plotted in Figure 3-20 – Figure 3-22 after the conversion to the wind axis coordinate system.
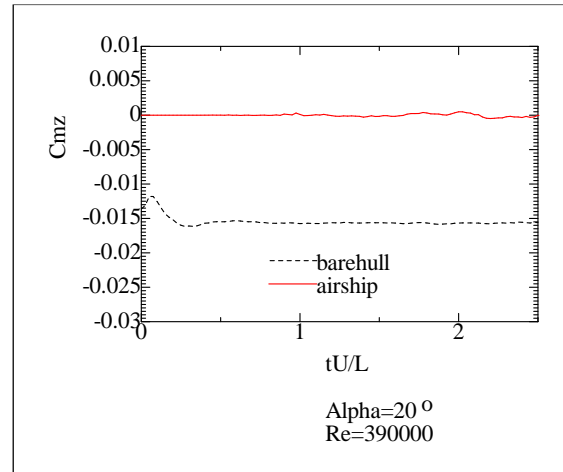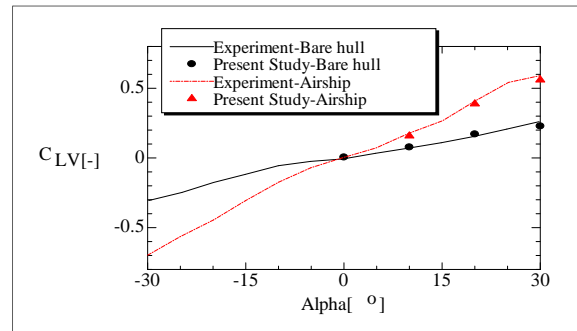

Figure 3-20: Comparison of the lift coefficient

Figure 3-20 shows a comparison of the computed and experimentally determined values of the volumetric lift coefficient. Both have a value of zero at an angle of incidence α = 0°. The computed values of the lift coefficient on the bare hull at an angle of incidence of 10° and 20° are in good agreement with the experimentally determined values though they are somewhat high. When the angle of incidence α = 30°, the computed results are close to the experimental results, but somewhat lower. This is because of fully complex separated flows. A comparison of the volumetric drag coefficient with the experimental results of Ref [T. Lutz, P. Funk, A. Jacobi, and S. Wagner, 2002] can be seen in Figure 3-21.
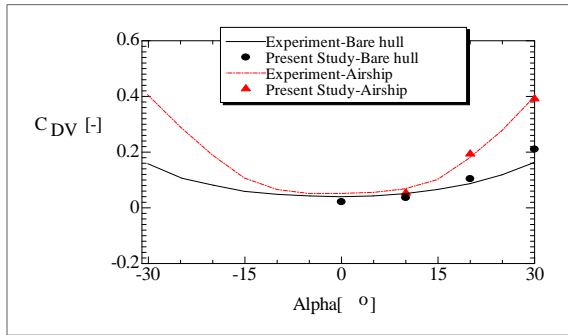
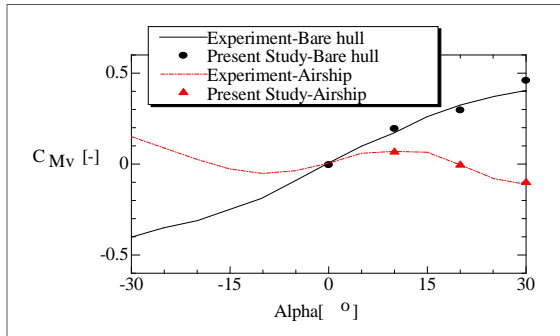Figure 3-21: Comparison of the drag coefficient

Figure 3-22: Comparison of the moment coefficient

The computed drag coefficient values are in good agreement with the experimental results. Figure 3-22 shows a comparison of the volumetric moment coefficient with the experimental results. Good agreement is also observed in this figure. General comparisons of the aerodynamic characteristics provide confirmation that the advance vortex method is a reliable tool for analyzing unsteady incompressible turbulent flows.

4   CONCLUSIONS

Numerical simulations of the unsteady flow around a bare hull and airship are carried out using the grid-free vortex method. Many flow phenomena are observed in the flow patterns such as horseshoes, vortex tips, and complex separated flow in the stern region. The pressure distribution on the surface and the aerodynamic characteristics are obtained. A comparison of the computed values of the aerodynamic characteristics

and experimentally determined one shows good agreement.

From the engineering point of view, it is reasonable to use this numerical method to develop and design new model airships and other vehicles.

REFERENCES

A. Leonard, 1980. *Vortex Methods for Flow Simulations*, J. Comp.Phys., 37, 289–335.

A. Ojima, and K. Kamemoto, 2000. *Numerical Simulation of Flow Around Three Dimensional Bluff Bodies by an Advance Vortex Method*, JSME, International Journal, 43, pp.127–135.

A.J. Chorin, 1973. *Numerical Study of Slightly Viscous Flow*, Journal of Fluid Mechanics, Vol. 57, pp. 785-796.

K. Fukuda and K. Kamemoto, 2004. *A Grid-Free Redistribution Model for a Vortex Method and Turbulent Flow Analysis*, Proceedings of the International Union of Theoretical and Applied Mechanics Symposium on Elementary Vortices and Coherent Structures: Significance in Turbulence Dynamics, Kyoto, Japan.

K. Kamemoto, 1995. *On Attractive Features of the Vortex Methods, in Computational Fluid Dynamics Review,* eds. M. Hafez and K.Oshima, JOHN WILEY & SONS, pp.334–353.

L. Rosenhead, 1931. *The Formation of Vortices from a Surface of Discontinuity*, Proceeding of the Royal society, A 134, pp170-192.

P.W. Bearmen, 1998. *Developments in the Understanding of Bluff Body Flow*, JSME International Journal, Series B, 41(1), pp.14–25.

T. Koumoutsakous, and A. Leonard, 1995. *High-resolution Simulations of the Flow Around an Impulsively Started Cylinder Using Vortex Methods*, Journal of Fluid Mechanics, 296:1-38.

T. Lutz, P. Funk, A. Jacobi, and S. Wagner, 2002. *Summary of Aerodynamic studies on the Lotte Airship*, 4th International Airship Convention and Exhibition, Cambridge, England.

T. Lutz, P. Funk, A. Jacobi, and S. Wagner, Aerodynamic Investigation on Inclined Airship Bodies.

T. Sarpkaya, 1989. *Computational Methods with Vortices–the 1988 Freeman Scolar Lecture*, ASME Journal of Fluid Engineering, 111, pp.5–52.